# Nanoscale Mechanical Characterization of Polymers by AFM Nanoindentations: Critical Approach to the Elastic Characterization

**ARTICLE** *in* MACROMOLECULES · MAY 2006

Impact Factor: 5.8 · DOI: 10.1021/ma052727j



**3 AUTHORS**, INCLUDING:

Davide Tranchida
Borealis
**37** PUBLICATIONS **472** CITATIONS
SEE PROFILE

Stefano Piccarolo
Università degli Studi di Palermo
**116** PUBLICATIONS **1,396** CITATIONS
SEE PROFILE

# Nanoscale Mechanical Characterization of Polymers by AFM Nanoindentations: Critical Approach to the Elastic Characterization

**Davide Tranchida,[†,‡] Stefano Piccarolo,*[,†,‡] and Maria Soliman[§]**

*Dipartimento di Ingegneria Chimica dei Processi e dei Materiali, Università di Palermo, Viale delle Scienze, 90128 Palermo, Italy, INSTM Udr Palermo, Palermo, Italy, and Sabic Europe, 6160 MD Geleen, The Netherlands*

*Received December 21, 2005; Revised Manuscript Received April 10, 2006*

ABSTRACT: AFM nanoindentations show a dependence of penetration, i.e., the relative motion between the sample and the tip (indenter), on material elastic properties when using the same load. This relationship becomes visible by using of samples being homogeneous down to the scale of nanoindentation. They were prepared from materials covering a broad range of mechanical behavior: from rubbery networks to glassy and semicrystalline polymers. The elastic modulus can be obtained applying Sneddon's elastic contact mechanics approach. To do this, some calibrations and instrumental features have to be measured accurately. All the polymers tested show that the contact between the tip and the sample is dominated by elastic behavior with negligible plastic deformation. In contrast to a standard metallic material like lead, the penetration dependence on load follows an exponent of 1.5, consistent with elastic contact mechanics. This can be justified on the basis of the large elastic range polymers exhibit, on the constraints due to the geometry of the deformation during indentation and to the critical yielding volume needed in order to induce plasticity. For the polymers studied, this volume is chosen in such a way that a significant material volume is irreversibly deformed. Elastic moduli taken from AFM force curves show a very good agreement with bulk values obtained by macroscopic tensile testing, on all the polymers tested. This result confirms that AFM nanoindentations in polymers take place mostly in the elastic range and opens the possibility to characterize the mechanical behavior of polymers on an unparalleled small scale compared to commercial DSI (depth sensing instruments), which use a much blunter indenter.

## Introduction

Physical properties of crystallizable polymers are determined by the morphology developed during solidification, i.e., the arrangement of crystalline domains and the resulting zones of intermediate order. Processing generates gradients of morphology so that the final properties are a complex combination of local features that are often difficult to identify and to relate to the conditions adopted during processing. Several parameters are the driving forces determining the morphology developed: high thermal gradients and pressures and orientations induced on the melt just before solidification. Morphology, mechanical properties and, if desired, processing conditions can be linked by atomic force microscopy (AFM) nanoindentation, because this technique allows the mechanical characterization on a morphological scale as well as the visualization of morphology on unparalleled scale. The tiny loads used cause deformation in the range of a few nanometers, allowing also the mapping of mechanical properties on inhomogeneous samples, thus measuring the properties of different phases on the submicrometer scale.

Microhardness,[1] a parent technique and one of the simplest methods used to measure mechanical properties of materials on a local scale, is rarely cited in connection with modulus determination. The impression left behind by the indenter is taken as a measure of plasticity, related to the yield stress, and, in the case of semicrystalline polymers, quantitatively related to crystallinity and crystal size.[2,3] The scale at which microhardness is measured is typical of the resolution of optical microscopes. Instrumented nanoindentation, measuring penetration depth continuously, while load is applied to the indenter, fills the gap between AFM nanoindentation and conventional microhardness.[4]

It is worth to mention that several other SPM-based techniques allow measuring surface stiffness.[5] Among others, dynamic approaches like, for example, atomic force acoustic microscopy (AFAM)[5−7] and ultrasonic AFM,[5,8,9] in which the AFM cantilever is vibrated at or near the frequencies of its resonant modes, resulting in a shift of the cantilever resonance frequencies, are perhaps the most promising. They are able to extract adhesive contact forces as well as the surface modulus.

AFM has proven to represent a useful tool to study mechanical properties on the nanometer scale, especially in biology[10−17] and polymer science.[18−29] AFM can indeed be used as a depth sensing instrument (DSI), recording the load applied on the tip, i.e., through cantilever deflection, and the relative motion between sample and tip, i.e., the penetration. The tip is used as an indenter instead of being scanned laterally across the sample surface. Under such conditions a force curve, i.e., a plot of penetration depth vs applied load, is recorded and then analyzed through contact mechanics models.[30−34] Limitations in the use of AFM as a nanoindentation tool arise first of all from the fact that the load is applied through a bending cantilever, because the normal commercial cantilevers are usually not stiff enough to indent metals and hard materials.[19,21] As a consequence only soft samples, mainly biological materials and polymers, have been analyzed. The strong point on using the AFM as a nanoindenter relies however on the fact that imaging the area to be indented becomes possible, and the shape and evolution of the indent imprint can be studied as a function of time.[29] Another important point is the versatility in the load range,

* Corrrsponding author. E-mail: piccarolo@unipa.it.
† Dipartimento di Ingegneria Chimica dei Processi e dei Materiali, Università di Palermo.
‡ INSTM Udr Palermo.
§ Sabic Europe.

10.1021/ma052727j CCC: $33.50 
Published on Web 05/25/2006

obtained by changing the cantilever stiffness, which can vary between fractions of a nanonewton up to a few tens of a micronewton.[28]

Despite the useful information the authors of the abovementioned papers[10−29] were able to extract about nanoscale mechanical properties, AFM nanoindentation is still thought to be a semiquantitative method.[35] Indeed, the AFM was not meant to perform nanoindentation, and if one uses it as a DSI instrument, it is necessary to tackle some experimental difficulties and calibrations. Furthermore, the choice of models for the specific mechanical behavior of polymers is crucial, and this will be explained in the following section.

Tip curvature radius, or, in some cases the overall tip geometry, has often been taken from producer data[11,13,16,17,24] not considering the production scattering Sometimes it has been measured by SEM even though the dimensions are on the order of 15 nm.[14] Sometimes the geometry is treated as an adjustable parameter in order to obtain results matching with macroscopic measurements.[23] The cantilever elastic constant has as well often been taken from producer data[11,13,14,16,17,24,26,27] or estimated on the basis of approximate methods.[23] Finally, in many circumstances it is not clear, if deflection sensitivity was, as prescribed, measured on a hard material.[15,16,19−24]

Other common constraints refer to the use of models without a clear contact mechanics basis. They are introduced for the purpose of improving the fitting of force curves; this approach has for example been used to analyze force curves of inhomogeneous materials.[14,16] In other approaches, a relative measurement was performed comparing the mechanical behavior of different samples,[26−28] while in some the Hertz model[30] was applied in a variety of situations when a fundamental assumption of this model was not satisfied.[12,15,19−23] Since, in general, it refers to the contact between two spheres, the link between applied load on a sphere (the indenter) and its penetration depth into a half-space (the sample) is obtained by setting one of the two radii in the original equation equal to infinite. A fundamental hypothesis for the model to be satisfied is that the radius of the contact must be much smaller than the sphere (indenter radius). Considering that the typical AFM tip has a curvature radius of approximately 10 nm, it is questionable whether this requirement can be satisfied. The effect of adhesion forces on the elastic modulus measurement has also been studied[20,21] even though these models are just corrections to the Hertz model in the case of the presence of adhesion forces, and thus intrinsically not applicable for AFM nanoindentation.

The Sneddon's elastic model can be used to study the contact of more complicated geometries than just a sphere, and the AFM tip can be approximated as a paraboloid. This approximation is satisfying if the tip shape is reasonably well represented by a paraboloid; due to the typical AFM tip shape, penetration depth must be smaller than approximately 120 nm, while larger penetration depths may be obtained at very tiny loads on very compliant materials. Characterization of these materials requires more complicated models where the indenter shape cannot be described by one of the simple geometries: a paraboloid, a sphere, or a cone. The model due to Segedin,[36] to our knowledge never used before in AFM nanoindentation studies, is using a series of polynomials to approximate the tip. It can provide more accurate predictions of the elastic modulus when used in conjunction with very compliant materials.

In this work raw force curves were collected on several polymer samples, covering a broad range of mechanical behavior: from a rubbery network, to several semicrystalline and amorphous materials. Calibrations and instrumental parameters were carefully determined, so that it was possible to translate this information into quantitative force vs penetration dependence. So we could study the contact mechanics and the peculiar mechanical behavior of polymers during indentations on nanometer scale in detail.

In the case of one of the polymers tested (iPP, isotactic polypropylene), homogeneous samples are solidified from the melt applying controlled cooling conditions in order to obtain a broad variety of morphologies and therefore of mechanical properties corresponding to different cooling rates.[37] High homogeneity of especially prepared rubbery networks,[38,39] gives the possibility to compare the Young's modulus, obtained from macroscopic tests, and the one calculated from instrumented indentation tests on the nanometer scale. The further link with local elastic properties is provided by a careful characterization of contact geometry through blind estimates.

## Experimental Section

The materials studied in this work were chosen to span a large range of mechanical properties (elastic moduli in the range of 7 MPa to 3000 MPa), corresponding to rubbers, semicrystalline and glassy polymers. They were further modulated, in the case of iPP, a semicrystalline polymer, by changing the morphologies. Those samples were obtained by a continuous cooling transformation, according to a procedure fully described elsewhere,[37] adopting solidification conditions from the melt spanning those, typically encountered in polymer processing, i.e., from a few degrees Celcius per second up to several hundreds of degrees Celcius per second. The samples obtained even at high cooling rates are homogeneous. They are also isotropic since solidification takes place in quiescent conditions.[37]

Poly(methyl methacrylate) (PMMA) was purchased from Aldrich with molecular weight, $M_w = 120\,000$. Poly(carbonate) (PC) was kindly provided by DSM with molecular weight, $M_w = 39\,000$. Isotactic poly(propylene) (iPP) was kindly provided by Montell. Its main characteristics were $M_n = 75\,100$, $M_w = 483\,000$, and $M_w/M_n = 6.4$. Low density poly(ethylene) (LDPE) was kindly provided by DSM. Poly(propylenglycole) (PPG) was purchased from Aldrich with a molecular weight of 725 and a dispersion index of 1.04. A commercial PTFE film, 50 $\mu$m thickness, was used as received from Goodfellow.

PMMA and PC samples were prepared using a hot stage (Mettler-Toledo FP82HT with FP90 central processor). IPP samples were prepared using four cooling rates (2.5, 25, 110, and 350 K/s) corresponding to the onset of the formation of the stable crystalline $\alpha$-monoclinic phase (2.5 K/s), decreasing in amount (degree of crystallinity) with cooling rate (25 and 110 K/s), up to 350 K/s where the onset of the formation of the metastable mesomorphic phase is observed.[37] PPG based rubber was synthesized by the authors according to the literature.[38,39]

The AFM used in this work is a Digital Instrument Nanoscope IIIA Multimode. The polymer morphology was studied in tapping mode at room temperature in the moderate tapping regime[40] ($0.6 < r_{SP} < 0.75$). Tapping silicon cantilevers (model TESP of Digital Instruments Inc. with a nominal cantilever elastic constant of 30 N/m; SNS18 and SNS14 of Micromasch with a nominal cantilever elastic constant of 40 and 3 N/m respectively) were used. Loads ranged from ca. 0.06 up to 4 $\mu$N. Although stiffer cantilevers could be used to expand the allowable loads range, most of the information on the mechanisms occurring are already obtained with the single standard cantilever.

A raw force curve is a plot of the voltage applied to the piezo vs the voltage output of the position sensitive diode (PSD) monitoring cantilever deflection. This can be turned into a more commonly used load−penetration depth curve if some experimental quantities are measured and some calibrations are performed. Quantities that were determined are deflection sensitivity, which allows one to turn voltage output from the PSD into cantilever deflection, cantilever elastic constant, which turns the latter into

applied load, and instrumental compliance. Deflection sensitivity was calculated, testing a very hard material. Under these conditions, the tip is not indenting the sample and the movement of the piezo equals the cantilever deflection. Cantilever elastic constant was estimated for each tip starting with the resonance frequency[41] of the cantilever and the measurement of cantilever geometry through SEM images.

Contact mechanics models can then be applied to the force curve if the geometry of the contact is known. The sample can be modeled as a half-space if roughness and thickness are respectively low and high enough. The typical roughness of the samples used is in this work, was in the order of a few nanometers on a $1 \times 1$ $\mu$m scale. The thickness was always much larger than 10 times the maximum penetration depth, so that no influence of the substrate is expected. Finally, the tip shape was estimated using the blind estimation technique.[42,43]

Nanoindentation was performed at frequencies in the range 0.01−33 Hz. Frequency is an experimental parameter that is *not* referring to dynamic mechanical testing. A voltage is applied to displace the piezo and the waveform is, to a good approximation, a saw tooth (with a certain frequency) if one excludes inertia effects which are frequency dependent and mostly located around the inversion point of the piezo scanning. Therefore, frequency is in this case related to loading rate. For example, a frequency of 10 Hz is equivalent to an indenter displacement rate of 18 $\mu$m/s for a piezo displacement of 900 nm. It is assumed that such rate is constant throughout the piezo scanning.

Macroscopic mechanical tests were performed in order to compare elastic moduli determined on nanometer scale by contact mechanics models with those of the bulk samples. DMTA measurements were performed in accordance with ASTM D5026 on RSA-II (Rheometrics Solids analyzer II) at a frequency of 1 Hz. Standard tensile test experiments were performed in a previous study on iPP using standard equipment (Instron testing machine model 1122).[18]

## Results and Discussion

The typical scale of the indentation is shown in this section. The experimental conditions enhancing elastic contact are identified on the basis of a comparison between penetration of the indenter during a force curve measurement and the residual imprint left upon unloading. This evidence is further justified comparing elastic moduli of the different materials tested with the values obtained by the loading part of force curves applying an elastic contact theory. This peculiar behavior is compared to the results obtained by larger scale tests, i.e., microhardness, and it is justified on the basis of many concurrent phenomena mostly recently reported in the literature. Finally evidence for a more accurate contribution of tip geometry is reported when indenting very compliant rubbery materials leading to large penetrations.

## Scale of the Indentation

Noncontact AFM mode with phase imaging provides direct access to the morphology without the need of surface pretreatment, (see Transmission Electron Microscopy). Operating in the so-called light tapping regime, the AFM can image the polymer surface nondestructively and resolve structures in the polymeric background. Figure 1 shows a PE sample where indentation tests have been performed at small distance from each other in order to allow the visualization of several indentation imprints in the same high-resolution image.

Figure 1 shows residual indentation imprints with exceptional morphological detail: to our knowledge, single crystalline lamellae bended by the indenter have never been shown before. The scale of the mechanical characterization through AFM nanoindentation is therefore clearly visible. A single or very few lamellae, upper right corner, can be tested as well as a bunch

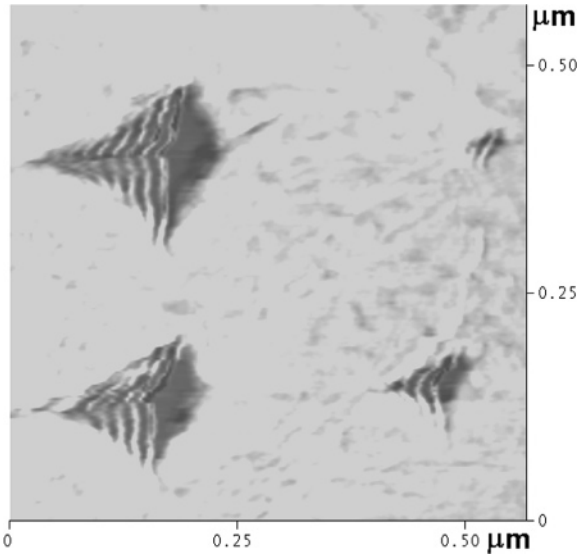


**Figure 1.** Residual indentation imprints on a PE sample after four indentations in the applied load range 0.6−4.8 $\mu$N. Single lamellae can be tested through indentations performed at tiny loads as well as several lamellae at larger loads.

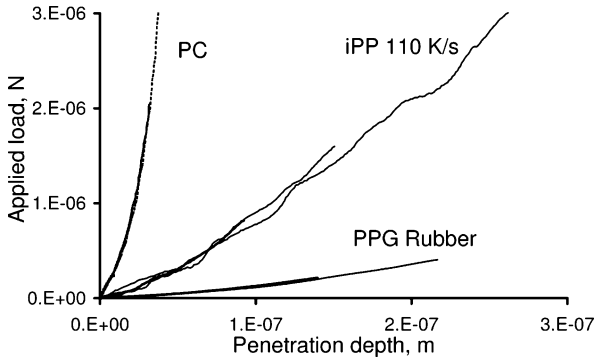


**Figure 2.** AFM force curves at three different maximum loads on three homogeneous polymer samples: PC, iPP solidified at 110 K/s and a PPG rubber. Low loads indentations are depicted with thicker lines.

of several lamellae depending on penetration. The possibility to push the characterization toward a morphological scale opens the way to link structure and mechanical properties through the characterization of the underlying components and their contribution to the macroscopic response. This objective can however be attempted only after developing the understanding of the mechanical behavior on an intermediate scale: small enough in order to achieve an in situ characterization of the special polymeric mechanical behavior on local scale, as explained in the Introduction, but large enough not to lose the continuum behavior. For these reasons, indentations were performed in this work at penetration depths sufficient in size to show a collective behavior of several lamellae and therefore an overall continuum behavior. More work is in progress for a full characterization at very small scale in order to reveal the contribution of each phase to the overall mechanical behavior and their complex interplay depending on morphological details.

The experimental data are presented, at first, in the form of applied load vs penetration depth curves. Figure 2 shows force curves collected on three materials at various applied loads, three for glassy PC and semicrystalline iPP and two for a PPG rubbery network. Force curves have been collected in random places on the sample, loads ranging from 0.2 to 3 $\mu$N pointing out the different mechanical behavior of these materials. The applied load − penetration depth curve is steeper for harder materials,

showing, as expected, smaller penetration depth at the same applied load, e.g. on comparing the penetration at 0.2 $\mu$N for PPG and PC or at ca. 3 $\mu$N for PC and iPP. The force curves are also continuous without pop-in events, i.e., discontinuities, which are usually related to fracture.[44] The study of cracks could strengthen this point: cracks were imaged, e.g., for PS indentations[45] but they are not visible in the AFM topography image of the indentation imprint on the materials studied in this work, neither in the AFM phase image, which is particularly sensitive to differences in material properties. This seems to suggest that no fracture takes place indenting at this load level and with this indenter geometry.

### Experimental Conditions for Elastic Contact

In a previous study, we have shown that the loading portion of the force curve from nanoindentation experiments is closely related to the elastic properties of the substrate being investigated.[13] This qualitative result is further investigated in this work mainly by identifying the conditions where negligible plastic and viscoelastic effects take place so that the elastic properties of polymers can be measured.

In the following we define as *indentation i* the depth of the tip residual imprint measured on the sample by a topographic scanning performed after the force curve is measured (i.e., an image collection), whereas we define *maximum penetration* $p_{max}$ as the tip maximum measured distance as registered during the measurement of the force curve obtained by using the AFM as a DSI. They differ because during unloading the sample partially recovers so that indentation is always smaller than the maximum penetration.

Usually, for polymer samples, indentation keeps on decreasing, eventually vanishing for very long times depending on sample characteristics. The viscoelastic recovery takes place for hours or days, and it can occur to a large extent suggesting that the residual indentation depth imaged by the AFM after indentation is not a plastic feature but mostly related to the material viscoelastic behavior. For example, it was shown for a PS with low molecular weight that the recovery is eventually complete even on time scales of a few hours.[29] Although this issue is going to be discussed further, for the moment we focus our attention on identifying some experimental conditions for which the contribution of plastic deformation is as low as possible. An elasticity parameter is then introduced, defined as

$$\xi = 1 - \frac{i}{p_{max}} \tag{1}$$

It approaches zero when there is no recovery (i.e., indentation is equal to maximum penetration), while it is one, when the elastic recovery is 100%. This is equivalent to introducing a dichotomy between two situations like long-term time dependent behavior that is equivalent to plastic deformation and short term to elastic deformation. The time responsible for the dichotomy is the experimental time between an indentation and the subsequent collection of the image. Although this simplification may seam rather crude it is justified, not only by the complexity of the stress field arising in indentations, but also by the materials tested, all of them being significantly far from any main thermodynamic transition.

The model PPG-based rubber shows exactly this behavior, Figure 3, the elasticity parameter being always equal to one. On the other polymers, the mechanical behavior is found to be different when indenting at different rates: usually the penetration depth decreases with increasing indentation rate.[18] In Figure 3, three more series of data are plotted, they refer to PMMA and to two iPP samples characterized by different morphologies. In all cases, the elastic parameter is low at low indentation rates, while it increases with increasing indentation rate eventually approaching a value of one at very high rates. We did not use the highest rate allowed by the AFM because inertia effects might start to be significant in the point of piezo motion inversion. We chose a frequency of 10 Hz throughout the rest of the work in order to maximize the elasticity parameter, $\xi$, and to keep it above 0.8 under the used conditions and for all the materials tested. The inset shown in Figure 3 clearly depicts this situation comparing the residual penetration, the thick mark as imaged by the AFM, to the plausible indent caused by the tip, represented by its shape, at the maximum load applied.

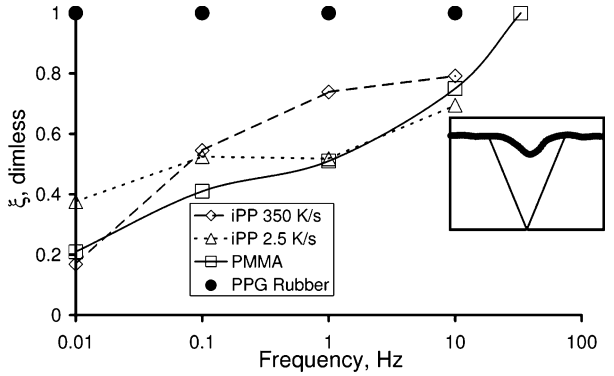


**Figure 3.** Dependence of the elasticity parameter on frequency for a wide range of materials behavior: from the PPG rubbery network to glassy PMMA and two iPP samples solidified at different cooling rates. The elasticity parameter is proportional to the elastic component of the deformation during a nanoindentation; see eq 1. The inset shows the residual penetration (thick profile) as imaged by AFM and the penetration depth under full load (thin profile) in the case of an indentation performed at 10 Hz, pointing out the large elastic recovery observed under this condition.

In the past, several papers dealing with AFM nanoindentation used a high loading rate to minimize viscoelastic effects without either quantifying the influence of plastic or long-term viscoelastic behavior or even without explaining such a choice. An exception is given by Tsukruk et al.,[19] who gave a guideline to relate the change in elastic modulus to the saw tooth wave applied to the piezo in order to bring the sample into contact with the tip during a force curve collection. Hochstetter et al.,[46] indenting on a micrometer scale, also showed that the behavior of PC and CR39 poly(diethylene glycol bis(allyl carbonate)) was strongly influenced by viscoelastic effects, so that, similar to our choice, the adopted high loading rates were used to isolate the elastic behavior and extract the Young's modulus.

### Comparison to Microhardness and Analysis of Micromechanics

It was already observed by Baltà-Calleja[2] that, during and after the indentation cycle, several different mechanisms take place: an elastic recovery of the material beneath the indentation upon removal of the load, a permanent plastic deformation, measure of microhardness, a time-dependent contribution during loading (creep), and a long-delayed recovery of indentation after load removal (viscoelastic relaxation).

From a mechanical standpoint, both amorphous layers and crystalline regions are deformed simultaneously due to continuity conditions under the applied compressive force, and crystallites remain more or less intact[47] on the initial quasi-elastic stages of indentation. However, at larger indentation times, with the disordered regions being highly compressed, the mechanical

properties are primarily governed by the plastic deformation of the crystals,[47] which results in yielding while the amorphous component behaves like a cross-linked (by crystallites) rubber, deforms elastically and transmits the stress to the crystals. Being the ratio of applied load and the projected area of the residual impression left behind the indenter, microhardness is a plastic property and indeed the close relationship to crystal size was soon recognized[1] and proven in a variety of conditions on quenched PE, slowly cooled from the melt PE, and for melt-crystallized paraffin.[48]

An empirical parallel model,[48] expressing the overall microhardness as the sum of the intrinsic contributions of crystalline and amorphous phases, allowed the authors to measure the hardness of the crystals from the hardness of the sample.[2,48] From this point on, extensive research has provided experimental evidence for a close relationship between microhardness and microstructure in polymeric materials[3,47,49] confirming the microhardness test as a useful structural probe.

According to the classic work of Tabor,[50] a stress analysis of the region under the indenter shows that almost two-third of the mean pressure is applied as a hydrostatic component and, hence, plays no role in producing plastic flow. This observation leads to the famous Tabor equation, relating the yield stress to approximately one-third of the microhardness. This fails when applied to polymers, because the elastic strains are not negligible.[3,51]

On the other hand, the phenomenology occurring in nanoindentation is fairly different from microindentation tests: this is due to the cumulative effect of several mechanisms, to be discussed in detail, the results shown in Figure 3 point to a negligible contribution of permanent deformations when the force curves are collected at high loading rates. This result is however quite surprising, because the AFM tip is a sharp indenter and it is well-known in the literature that a sharp indenter induces high localized stresses in the sample during the indentation, thus likely introducing plastic deformation.[52,53]

Concerning the amorphous polymers studied in this work, PC and PMMA below their glass transition temperature, the main mechanisms of plastic deformation are usually started by cavitation which subsequently boosts further crazing and shear yielding.[54] However, positive pressure components[55] arising during compression deformation, such as nanoindentation, prevent the formation of cavities and therefore a situation for maintaining the strength of the material is induced. It is worth to notice that yield however takes place at some point even without cavitation; due to strain induced softening, which lowers the glass transition temperature of the material involved by the stress field and then allows segmental motion of the chain resulting in macroscopic yielding.[54] Due to the larger stress level at which this yielding mechanism takes place, the mechanical contact between the AFM tip and the sample may take place in the prevailing elastic range, as shown by the points at high frequency of Figure 3 belonging to PMMA.

Cavities occurring in the amorphous layers connecting crystallites are also frequently responsible for yield of semicrystalline polymers in tension. As abovementioned, cavitation is strongly inhibited during nanoindentation even though there can be some small volumes subjected to tensile deformation. However, Pawlak and Galeski[56] showed that typical dimensions of stable cavities for iPP and HDPE, two materials studied in this work, lie in the range of 22−40 nm while the smaller ones are immediately healed.[56] The occurrence of cavities with size comparable to the entire volume deformed by nanoindentation is therefore highly unlikely. This means, when comparing to drawn samples, compression produces elastic deformation to a much larger true strain and respond with a much larger true stress[56] as compared to tension. As a result, yield stress and yield strain are significantly larger for compression.

This condition is even enhanced for nanoindentation due to the possibility to take advantage of a size scale effect as described by Bushby and Dunstan.[57] It is physically plausible that yielding, and thus plasticity, takes place when the yield stress has been reached in a critical finite volume, where it starts cooperatively rather than in one point only, as the common yielding criteria assume. When indenting with blunt tips, as in microhardness tests, the stress field does not change very quickly, so it can be assumed that the yield stress is reached in the same moment throughout a volume larger than the critical one. If sharp indenters are used, a very high maximum local stress must be reached in order to induce plasticity. Since the stress changes very quickly at small distance from the point where it is at a maximum level, the local stress is already below the yield threshold. To quantify this dimension, Bushby and Dunstan[57] reported a criterion for which this size scale effect occurs when the ratio $\lambda = R^2/r_0^2$ is close to the ratio $\zeta = E/\sigma_Y$, the elastic modulus and the yield stress of the material. Here $R$ is the tip radius and $r_0$ is the radius of the critical volume assumed to be a sphere. The critical volume radius comes out to be approximately 1 nm, if we assume that the size scale effect takes place when $\lambda$ and $\zeta$ are equal, where $\zeta$ is approximately 50 for polymers and the typical tip radius is 5−10 nm. This estimate is also in good agreement with recent experimental results[58] showing that the critical yielding volume, needed to induce a size scale effect, of an iPP sample has been figured out to be around 4.8 $(nm)^3$, while it is slightly smaller for PC[59] and PMMA,[60] i.e., on the order of 3.3 $(nm)^3$. The relation between the critical volume and morphological parameters is stated in the literature;[61] however, this discussion is beyond the scope of this work.

Moreover, yielding of semicrystalline polymers is crystallographic in nature and is started by the onset of crystal slips which relax the stress when it reaches the level sufficient for triggering the easiest crystallographic slip along the direction of the chain, the [001] in the case of iPP. It is worth to notice that the easiest crystallographic slip for iPP (010)[001] takes place at a critical resolved shear stress of about 22−25 MPa along the direction of the chain,[62] and it means that, depending on the orientation of the lamellae, the real yield stress can reach values as high as 50−55 MPa.[56] The collective action of the slips leads then to the macroscopic yielding[63,64] and, from a micromechanics point of view, to the rotation of the chain axis toward the flow direction accompanied by rotation of lamella from the perpendicular to the parallel loading direction.[63−65] An even larger stress might be expected for the activation of this process in the extremely small volume beneath the AFM tip, because of the size scale effect and the probably difficult rearrangement of the lamellae within the very tiny volume subjected to the high stress field. This may explain the reason for a prevailing elastic response observed for semicrystalline polymers.

The crucial concept that, in the case of polymers, indentations take place in the elastic range while micromechanical plastic phenomena can be neglected is the central issue of this work. Although a touch of this behavior was already suggested by our previous work,[18] a more systematic set of evidences is provided here. These circumstances together with the unavailability of the true deformation field and the size scale effect do not cast doubts on the possibility that the behavior is indeed

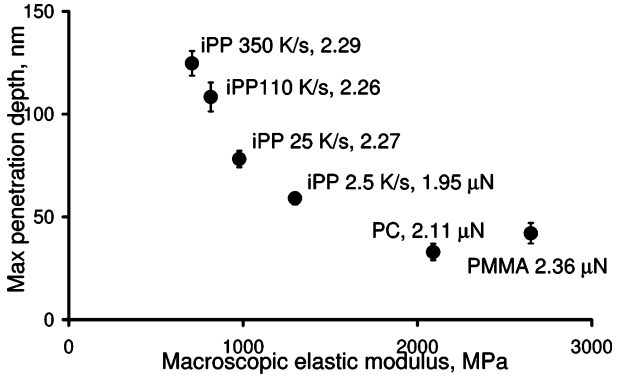


**Figure 4.** Maximum penetration depth at similar applied loads vs macroscopic elastic modulus measured by bulk tensile testing.

apparently or substantially elastic or, which is the same thing, that an overall elastic contact theory fits the force curve data and allows us to extract an elastic modulus in agreement with the value drawn from macroscopic tests, i.e., of the bulk material.

### Modeling Contact Mechanics

A first experimental proof is given by the qualitative relationship between maximum penetration depth and elastic modulus, obtained by a macroscopic tensile testing machine, shown in Figure 4. When performing indentations with the same applied load on different samples, a different penetration depth is obtained immediately pointing to the different elastic properties of the materials.

Figure 4 shows this relationship for four iPP morphologies and for PC and PMMA. The macroscopic elastic modulus, $E_M$, has been put on the *x*-axis in order to show the existence of a relationship with the penetration depth although the applied load was not strictly kept constant during nanoindentation. Since the relationship suffers from some scattering, the applied load has also been specified in the figure in order to justify deviations from the underlying monotonic trend.

Although Figure 4 clearly points out the qualitative relationship of the elastic modulus with the penetration depth determined from nanoindentation, the arguments previously reported suggest that a quantitative approach can be attempted, based on contact mechanics models.

In a previous work[66] it was shown that the unloading curve of AFM nanoindentations cannot be used to extract information about Young's modulus through the commonly used Oliver and Pharr analysis.[67] The root of this procedure, i.e., the Sneddon's elastic contact analysis, is indeed in disagreement with the experimental results.[66] The reason for this deviation can be identified by the role of the polymeric viscoelastic behavior during the unloading process. The procedures reported in the literature to minimize its contribution[46] are not sufficient to improve the results. Concerning the contact geometry, the use of a tip (opening angle of ca. 90° and radius of curvature in the order of a few tens of a nanometer) blunter than the one commonly used in AFM experimental conditions (opening angle of ca. 30° and tip radius on the order of 5−10 nm) does not improve the situation as well.[66] The same is true in the case of commercial nanoindenters, where the use of a standard Berkovich indenter (opening angle of ca. 141° and radius of curvature in the order of hundreds of nanometer) casts doubts about the use of all the methods reported in the literature to analyze the unloading curves, starting from Sneddon's purely elastic contact mechanics approach.

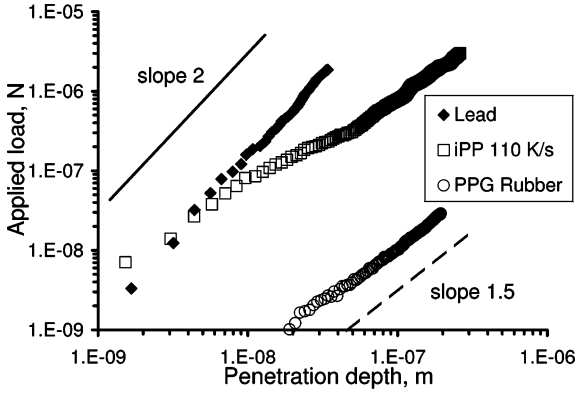


**Figure 5.** Logarithmic plot of applied load vs penetration depth collected on two polymer samples: a PPG rubber and an iPP sample solidified at 110 K/s. The typical slope of 1.5 is compared to a metal sample, lead, for which a slope of 2 is measured.

On the other hand, the loading curve is supposed to show, for ceramics and metals, the elastic-plastic behavior of the material.[68] Loubet et al.[68] have attempted an elastic-plastic approach requiring for the loading curve a power law relation between load and penetration depth, the exponent being equal to 2 in the case of a conical indenter. The quadratic scaling relation was also confirmed for more complicated mechanical behavior, since it takes into account the strain-hardening behavior.[69]

An alternative uses a dimensional analysis of the indentation quantities[70] involved in a conical indentation of an elastic−plastic material with strain hardening which, for indentations in the nanometer scale, must introduce a length scale due to the fact that a perfectly sharp indenter is not realistic under such conditions. The following dimensionless equation can then be drawn

$$\frac{F}{Ep^2} = \Pi\left[\frac{l}{p}, \frac{\sigma_Y}{E}, n, \theta\right] \tag{2}$$

making the exponent, which scales applied load and penetration depth, to deviate from two. The strain hardening exponent *n*, indenter opening angle $\theta$ and the length scale *l* are the relevant quantities in eq 2. The length scale *l* can be identified by modeling the tip as a paraboloid of revolution, which, in cylindrical coordinates, is

$$\rho^2 = 4qz \tag{3}$$

where *q* is a constant proportional to the curvature. In this case the length scale is represented by the curvature radius at the apex which, from eq 3, is equal to 2*q*.

The solution for the elastic contact, given by Sneddon[34] satisfies both, the need to introduce a length scale and an exponent smaller than 2 in[34]

$$F = \frac{4E}{3(1-\nu^2)}(2qp^3)^{1/2} \tag{4}$$

showing that load scales with penetration depth with an exponent of 1.5. Since the theory deals with an elastic contact, it adequately describes, in Figure 5, the force curve shape in the case of the PPG rubber (for which $\xi$ is equal to 1) while it fails in describing the behavior of an elastic-plastic material, i.e., lead. As expected, the two force curves show different slopes in a logarithmic penetration depth vs applied load plot. They

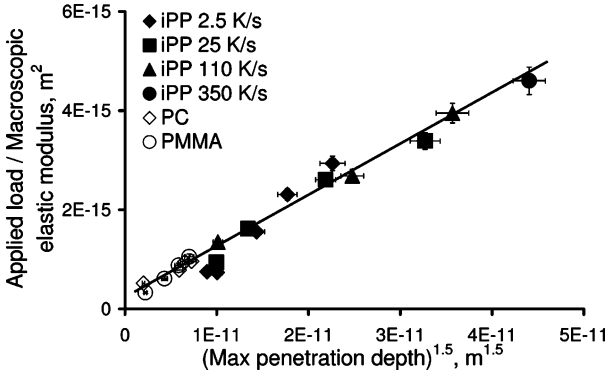


**Figure 6.** Dependence of the applied load, normalized by elastic modulus measured through bulk tensile tests, on maximum penetration depth to the power of 1.5 for several samples covering a very broad range of elastic properties. For iPP the solidification conditions are reported in terms of cooling rate, K/s.

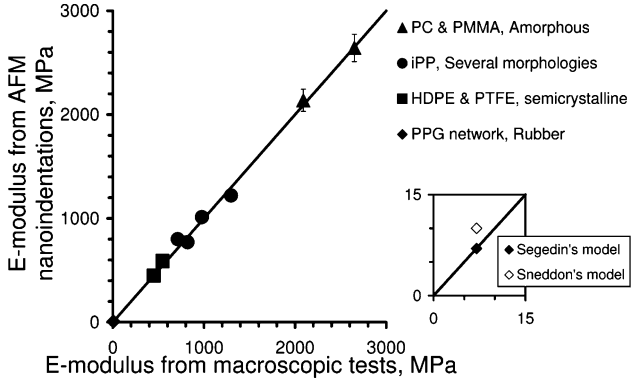


**Figure 7.** Comparison of the elastic modulus drawn from AFM nanoindentations by the Sneddon's elastic contact model, eq 5, with the so-called macroscopic one obtained from bulk tensile testing. Here all the samples tested in this work are reported, covering a very broad range of elastic properties.

are linear, confirming power law relations, but slopes are different and almost equal to 1.5 for the PPG rubber and 2 for lead.

It was shown in Figure 3 that it is possible, for the polymers studied in this work, to find conditions where the mechanical defomation is mostly taking place in the elastic range. Under these experimental conditions the Sneddon model adequately describes the shape of the force curves, as shown in Figure 5, where a typical force curve is plotted for an iPP sample to compare the behavior with the two model materials. The slope is in this case equal to 1.5, confirming the results pointed out in Figure 3 when using high indentation rates.

This result is also confirmed by Figure 6 where applied load, normalized by macroscopic elastic modulus, is plotted vs maximum penetration depth to the power of 1.5. To avoid confusion in this figure, each point represents a force curve, relating applied load and maximum penetration depth for all the materials studied (PMMA, PC, four different iPP morphologies). A straight line fits the data although some scattering may be introduced due to the variation in tip radii of the different cantilevers used. Figure 6 suggests that the predictions of Sneddon's model are adequate to describe the mechanical behavior of the polymers analyzed in this work through nanoindentation performed by AFM and therefore that the contact between tip and material takes place mostly in the elastic range.

It is unfortunate that several publications[10−29] chose an involvement with ill defined contact mechanics, i.e., with a wrong interpretation of Hertz theory as explained in the following, or procedures without a clear theoretical basis.

A common approach consists of the application of Hertz theory to load−penetration experimental data to work out the Young's modulus of the material tested. Hertz theory is thought to be an exact solution for the contact of a rigid sphere indenting an elastic half-space, valid only at small displacements. This is a serious limitation for AFM nanoindentation, because the tip is very sharp ($R$ approximately 5−20 nm) and contact areas are much smaller than the tip radius, using this hypothesis, are almost immeasurable. Surprisingly, this method allows the accurate evaluating of the elastic modulus under conditions where Hertz assumptions are not met, i.e., contact radii of the same order or even larger than indenter radius, even though this fact was rarely or never pointed out. Examining the more complete Sneddon's derivation for general indenter shapes, one may easily understand that Hertz results do not fit with the general solution for the spherical indenter, while they do fit with the one for the parabolic indenter. The applicability of Hertz solution to AFM nanoindentation originates then on the point that Hertz solution is, more correctly, a general solution for the parabolic punch[34] that can be valid also for a sphere when it can be approximated by a paraboloid, i.e., at small displacements.

Following this discussion, previous contributions[10−29] should be seen as the application of Sneddon's theory, without any limitation on penetration depth and with the only limitation that this theory relies on classical elasticity theory neglecting altogether viscoelastic or plastic contributions.

Once stated that the elasticity parameter $\xi$ suggests the contact to be mainly elastic and that the force curve exponent confirms the applicability of Sneddon's model, a further check is possible on the physical meaning of the proportionality factor scaling applied load and penetration depth to the power of 1.5, i.e., whether it allows getting information about material properties. Such proportionality factor contains some geometrical parameters as well as mechanical properties, elastic modulus being the most important.

The materials used in this work are characterized by high homogeneity so that there are no reasons to expect a different behavior on macro- or nanometer scale, allowing comparing results of elastic modulus measurements obtained by macroscopic tensile tests and those from AFM nanoindentation.[18] An agreement between the elastic modulus determined by nanoindentation through the application of Sneddon's model, and the macroscopic one would be a further evidence of the fact that Sneddon's model may be used, besides being a proof of the AFM as a useful tool for mechanical characterization on the nanometer scale. The moduli determined by nanoindentations and the use of Sneddon's model are plotted in Figure 7. The 1:1 plot shows that they are very close to the elastic moduli determined on the bulk, pointing out the possibility to perform in situ mechanical analysis with a very high lateral resolution, i.e., being available by AFM.

The agreement between the bulk and the near-surface data for PMMA and PC seems to suggest that no surface glass transition effects are observed by means of AFM nanoindentation on a 10−40 nm length scale on these glassy systems. Although there is still much debate in the literature[71−76] on the length scale, where an increase of mobility and therefore a decrease of glass transition is observed, it is surprising that surface glass transition effects are sometimes discussed on a much larger scale, hundreds of nanometers, to explain the

dissimilarity between FEM simulated force curves and experimental ones.

The agreement is also registered for intrinsically inhomogeneous samples as all the semicrystalline materials like HDPE, PTFE, and the iPP's, solidified at different cooling rates, used during this investigation. This observation requires not only that the morphology developed is homogeneous throughout the sample thickness,[32] it also implies that the material behavior on the scale of 10−40 nm is the same as in the bulk. Therefore, the peculiarities arising from the morphology, i.e., from the texture of the multiphase material, do not show up individually and the material response is that of a continuum. This should not be surprising on the basis of the interaction observed between the nanoindenter and the crystalline lamellae, clearly observed in Figure 1, where a bunch of crystallites is involved in the deformation. It would be interesting to investigate the minimum indentation length scale down to which the continuum-like behavior is observed. Preliminary results show that upon further decreasing the applied load, the distribution of elastic moduli observed when performing a statistical analysis of the obtained values, spreads out eventually, showing a bimodal or even multimodal behavior. The difficulty of such measurements, still in progress, lies in obtaining melt solidified samples with a surface finish, which unambiguously rules out the possibility that the spread of the results does not depend on sample roughness.

### Modeling Contact Mechanics at Large Penetration Depth

Even though the results presented up until now, strongly provide evidence for an elastic response that can be modeled using the Sneddon's model, some further remarks need to be pointed out. The approximation of the indenter shape with a paraboloid, suggested by the exponent relating applied load to penetration depth, as shown in Figure 6, leads to a correct evaluation of Young's modulus in Figure 7. However, modeling the tip with a paraboloid can still be a rude approximation for larger penetration depths. The empty diamond of the inset in Figure 7 shows that very compliant materials, such as the PPG-based rubbers are, need a different approach to evaluate the Young's modulus through nanoindentation. The reasoning behind this statement lies in the fact that the penetration depth obtained at tiny loads is already so large that the paraboloid approximation for the AFM tip is not satisfactory. A more precise solution can be obtained using the Segedin's[36] approach for the mechanical contact, to our knowledge never adopted in previous work, leading to a correct evaluation of the Young's modulus of compliant materials as shown by the filled diamond in the inset of Figure 7.

Segedin[36] found the relation between penetration depth and applied load for an indenter of arbitrary profile when it can be modeled by a series:

$$z = \sum_{n=1}^{+\infty} c_n \rho^n \tag{5}$$

Penetration depth is then evaluated for a known contact radius, $a$,

$$p = \sqrt{\pi} \sum_{n=1}^{+\infty} \frac{\Gamma(1/2n+1)}{\Gamma(1/2n+1/2)} c_n a^n \tag{6}$$

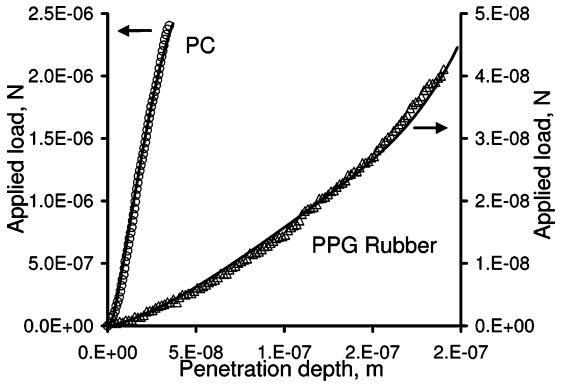


**Figure 8.** Fitting of two force curves, obtained by the Segedin[36] contact model, eqs 6 and 7, compared to experimental data referring to two extreme cases: the rubber PPG network and the PC sample.

At the same contact radius $a$, the applied load is evaluated as well through

$$L = \frac{2\sqrt{\pi}\mu a}{1-\nu} \sum_{n=1}^{+\infty} \frac{\Gamma(1/2n+1)}{\Gamma(1/2n+1/2)} c_n a^n \tag{7}$$

where $\mu$ is the Lame' coefficient.

A force curve relating penetration depth and applied load is then derived by coupling these two values, obtained at the same contact radius, once the indenter profile is known. This can be assumed to be a sphere near the apex, measured through blind estimation, and conical with an opening angle arising from technological constraints during tip manufacturing. Continuity of the derivative between the two geometries gives an accurate description of the AFM tip profile with the series in eq 5 cut after the 16th term. A force curve of a compliant PPG-based rubber and a stiff PC sample can be fitted with eqs 6 and 7, as shown in Figure 8. The only fitting parameter is Young's modulus, which is shown to be 7 MPa for the PPG-based rubber and 1.99 GPa for PC. The latter is very similar to the value calculated by Sneddon's approach since in this case the penetration depth is so small that a paraboloid modeling of the AFM tip is adequate.

The use of Segedin's approach, to model the contact between a complex shape tip and the sample, does not violate any theoretical hypothesis, like the Hertz model does, and it did not suffer from limitations on penetration depth as the Sneddon's model. The only constraint is that classical elasticity theory must hold. In the case of polymers this can be satisfied once it is possible to identify experimental conditions which meet this requirement, i.e., that the indentation takes place at true nanometer scale. This is being done by using the polymers investigated in this work with a large elastic range.

### Conclusions

The Atomic Force microscope can be used as a depth sensing instrument to collect force curves. This is possible although the dependence of the measured force on the relative motion between the indenter, the tip, and the sample requires several calibrations and preliminary determinations in order to turn a force curve into a reproducible plot of force vs penetration depth, which is able to distinguish differences between materials and their mechanical behavior. In this way true nanometer scale indentations can be obtained due to the low loads. These can be furthermore varied in a broad range by just changing the

cantilever elastic constant. Low loads and consequent low penetration depths imply very good lateral resolution, which might be very useful for mapping mechanical properties of inhomogeneous materials. Typical AFM cantilevers are however not stiff enough (too compliant) to be used to indent hard materials, and this method turns out to be particularly useful for soft materials like polymers and biological materials.

In this work, indentations were collected on several polymers with mechanical properties spanning a broad range; from a rubbery network of controlled texture to two amorphous polymers (PC and PMMA) and also several semicrystalline materials: HDPE, PTFE, and iPP. The latter was solidified from the melt under controlled cooling rates, which gave rise to different degrees of crystallinity of the stable α-monoclinic phase and also to the mesomorphic morphology at the largest cooling rates adopted. In every case much care was taken to obtain a homogeneous isotropic structure, keeping the properties constant throughout the sample.

In the case of the rubber sample, indentation is completely reversible, and the residual imprint, measured through images collected after each indentation, is negligible. For the other polymers, suitable testing conditions can be identified where the residual imprint is up to five times smaller than the maximum penetration depth under load, showing a significant short time elastic recovery.

In standard DSI, the initial unloading slope is usually assumed to be related to the elastic modulus although in the case of polymers we have recently pointed out the limitations of this approach in the case of AFM force curves. On the opposite the loading portion of the force curve should give rise to a complex stress field, highly three-dimensional, with large gradients leading to irreversible deformations.

In the case of all the polymers investigated, the mechanical behavior in the loading portion of the force curve is dominated by an elastic response with a close relation of the penetration depth on the material's macroscopic elastic modulus at constant load. The applied load is scaling with the penetration depth for all the polymers investigated exactly like a rubber, and it obeys elastic contact models like the one from Sneddon, who is assuming that the tip can be described as a paraboloid with the radius of curvature equal to that determined by blind estimation.

This behavior is attributed to several distinct and probably synergetic phenomena: certainly the large elastic range, typical for polymeric materials,[56,62−65] which, when accompanied by the confinement determined by the volume around the indentation,[55] induces side constraints which enforce the deformation,[56,63−65] especially in the case of a compression geometry, where the absence of cavitation significantly extends the elastic range.[56] Also the use of a sharp indenter, like the one used in AFM cantilevers, takes advantage of size effects, especially in polymers, to enhance the elastic behavior. Even though a sharp indenter induces high stresses in the volume tested,[52,53] the stress field is rapidly changing and only a small volume of the material experiences a stress higher than the macroscopic yield stress. If such volume is smaller than a critical value,[57] it will not give rise to the onset of plasticity, and therefore, the indentation is dominated by elastic deformations.

The elastic modulus determined by indentations with loads in the order of a few $\mu$N is very similar to the bulk elastic modulus for a wide range of values, from the rubber used, in the range of 10 MPa, up to PC with a modulus of ca. 2 GPa. In the range of maximum penetration depths tested, of ca. 15−50 nm, moduli of amorphous polymers coincide with bulk values suggesting that at such length scales no significant increase of surface mobility takes place, which would decrease the $T_g$ and consequently the elastic modulus. For very compliant materials, i.e., the rubber adopted in this work, penetration depths are very large, such that describing the tip as a paraboloid may be a source of inaccuracy. Indenters of arbitrary profile can however be described, always assuming perfect elastic contact, by an approach based on Segedin,[36] improving significantly the prediction of elastic moduli for large penetration depths.

In all cases considered in this work, the material is assumed to behave as a continuum, and on the scale of indentations with penetration depths of 15−50 nm, mechanical properties are assumed to be representative of the bulk. The assumption is clearly confirmed by the good agreement with bulk moduli measured on macroscopic samples with homogeneous morphology. Recent results however show that upon a significant decrease in the applied load and, consequently, the penetration depth, moduli of semicrystalline iPP solidified at different cooling rates become very scattered with a statistical distribution departing from a monomodal behavior. Although the dependence on texture, applied load, and mechanical properties of the material are still under investigation, there is a clear potential to discriminate properties of component phases and their mutual connectivity.

**Acknowledgment.** The authors acknowledge the financial support of the PhD grant of D.T. by the University of Palermo and the financial support from the Italian Ministry of University and Scientific Research (MIUR, Italy), PRIN04 grant. D.T. is grateful to Dr. R. Deblieck and Dr. R. Kleppinger of DSM Research for their continuous assistance and stimulating suggestions during his permanence at the DSM research center in Geleen, The Netherlands, and to Dr. L. Boscarol and Dr. E. Sperotto of DSM Research for the synthesis of the PPG-based rubbers.

## References and Notes

(1) Baltà-Calleja, F. J. *Adv. Polym. Sci.* **1985**, *66*, 117.
(2) Baltà-Calleja, F. J. *Trends Polym. Sci.* **1994**, *2*, 419.
(3) Flores, A.; Baltà-Calleja, F. J.; Attenburrow, G. E.; Bassett, D. C. *Polymer* **2000**, *41*, 5431.
(4) Van Landingham, M. R. *J. Res. NIST* **2003**, *108*, 249.
(5) Loos, J. *Adv. Mater.* **2005**, *17*, 1821.
(6) Cuenot, S.; Fretigny, C.; Demoustier-Campagne, S.; Nysten, B. *J. Appl. Phys.* **2003**, *93*, 5650.
(7) Rabe, U.; Amelio, S.; Kester, E.; Scherer, V.; Hirsekorn, S.; Arnold, W. *Ultrasonics* **2000**, *38*, 430.
(8) Yamanaka, K.; Noguchi, A.; Tsuji, T.; Koike, T.; Goto, T. *Surf. Interface Anal.* **1999**, *27*, 600.
(9) Inagaki, K.; Matsuda, O.; Wright, O. B. *Appl. Phys. Lett.* **2002**, *80*, 2386.
(10) Yao, X.; Walter, J.; Burke, S.; Stewart, S.; Jericho, M. H.; Pink, D.; Hunter, R.; Beveridge T. J. *Colloids Surf. B: Biointerfaces* **2002**, *23*, 213.
(11) Yamada, T.; Arakawa, H.; Okajima, T.; Shimada, T.; Ikai, A. *Ultramicroscopy* **2002**, *1*, 261.
(12) Charras, G. T.; Lehenkari, P. P.; Horton, M. A. *Ultramicroscopy* **2001**, *86*, 85.
(13) Maxwell, J. M.; Huson, M. G. *Micron* **2005**, *36*, 127.
(14) Rabinovich, Y.; Esayanur, M.; Daosukho, S.; Byer, K.; El-Shall, H.; Khan, S. *J. Colloid Interface Sci.* **2005**, *285*, 125.
(15) Liang, X.; Mao, G.; Ng, K. Y. S. *J. Colloid Interface Sci.* **2004**, *278*, 53.
(16) Sato, M.; Nagayama, K.; Kataoka, N.; Sasaki, M.; Hane, K. *J. Biomechanics* **2000**, *33*, 127.
(17) Lieber, S. C.; Aubry, N.; Pain, J.; Diaz, G.; Kim, S.-J.; Vatner, S. F. *Am. J. Physiol. Heart Circ. Physiol.* **2004**, *287*, H645.
(18) Tranchida, D.; Piccarolo, S. *Polymer* **2005**, *46*, 4032.
(19) Tsukruk, V. V.; Gorbunov, V. V.; Huang, Z.; Chizhik, S. A. *Polym. Int.* **2000**, *49*, 441.
(20) Chizhik, S. A.; Huang, Z.; Gorbunov, V. V.; Myshkin, N. K.; Tsukruk, V. V. *Langmuir* **1998**, *14*, 2606.

(21) Tsukruk, V. V.; Huang, Z.; Chizhik, S. A.; Gorbunov, V. V. *J. Mater. Sci.* **1998**, *33*, 4905.
(22) Shulha, H.; Kovalev, A.; Myshkin, N.; Tsukruk, V. V. *Eur. Polym. J.* **2004**, *40*, 949.
(23) Cappella, B.; Kaliappan, S. K.; Sturm, H. *Macromolecules* **2005**, *38*, 1874.
(24) Fang, T.-H.; Chang, W.-J.; Tsai, S.-L. *Microelectron. J.* **2005**, *36*, 55.
(25) Raghavan, D.; Gu, X.; Nguyen, T.; VanLandingham, M.; Karim, A. *Macromolecules* **2000**, *33*, 2573.
(26) VanLandingham, M. R.; Dagastine, R. R.; Eduljee, R. F.; McCullough, R. L.; Gillespie, J. W. *Composites: Part A* **1999**, *30*, 75.
(27) VanLandingham, M. R.; McKnight, S. H.; Palmese, G. R.; Eduljee, R. F.; Gillespie, J. W.; McCullough, R. L. *J. Mater. Sci. Lett.* **1997**, *16*, 117.
(28) Cappella, B.; Dietler, G. *Surf. Sci. Rep.* **1999**, *34*, 1.
(29) Karapanagiotis, I.; Evans, D. F.; Gerberich, W. W. *Polymer* **2002**, *43*, 1343.
(30) Landau, L. D.; Lifshitz, E. M. *Theory of Elasticity*; Pergamon Press: Oxford, U.K., 1986.
(31) Derjaguin, B. V.; Muller, V. M.; Toporov, Y. P. *J. Colloid Interface Sci.* **1975**, *53*, 314.
(32) Johnson, K. L.; Kendall, K.; Roberts, A. D. *Proc. R. Soc. London* **1971**, *A324*, 301.
(33) Maugis, D. *J. Colloid Interface Sci.* **1992**, *150*, 243.
(34) Sneddon, I. N. *Int. J. Eng. Sci.* **1965**, *3*, 47.
(35) Pratt, J. R.; Smith, D. T.; Newell, D. B.; Kramar, J.; Whitenton, E. *J. Mater. Res.* **2004**, *19*,.
(36) Segedin, C. M. *Mathematika* **1957**, *4*, 156.
(37) Brucato, V.; Piccarolo, S.; La Carrubba, V. *Chem. Eng. Sci.* **2002**, *57*, 4129.
(38) Steeman, P. A. M.; Nusselder, J. J. H. *Polym. Gel Networks* **1995**, *3*, 159.
(39) Bos, H. H.; Nusselder, J. J. H. *Polymer* **1994**, *35*, 2793.
(40) Garcìa, R.; Pérez, R. *Surf. Sci. Rep.* **2002**, *47*, 197.
(41) Green, C. P.; Lioe, H.; Cleveland, J. P.; Proksch, R.; Mulvaney, P.; Sader, J. E. *Rev. Sci. Instrum.* **2004**, *75*, 1988 and references therein.
(42) Villarrubia, J. S. *Surf. Sci.* **1994**, *321*, 287.
(43) Villarrubia, J. S. *J. Res. NIST* **1997**, *102*, 425.
(44) Morris, D. J.; Myers, S. B.; Cook, R. *J. Mater. Res.* **2004**, *19*, 165.
(45) Van Melick, H.; Bressers, O.; den Toonder, J.; Govaert, L.; Meijer, H. *Polymer* **2003**, *44*, 2481.
(46) Hochstetter, G.; Jimenez, A.; Loubet, J. L. *J. Macromol. Sci., B: Phys.* **1999**, *38*, 681.
(47) Baltà-Calleja, F. J.; Flores, A.; Ania, F.; Bassett, D. C. *J. Mater. Sci.* **2000**, *35*, 1315.
(48) Baltà-Calleja, F. J.; Kilian, H.-G. *Colloid Polym. Sci.* **1985**, *263*, 697.
(49) Flores, A.; Baltà-Calleja, F. J.; Bassett, D. C. *J. Polym. Sci. B* **1999**, *37*, 3151.
(50) Tabor, D. *Hardness of Metals*; Oxford University Press: London, 1951.
(51) Baltà-Calleja, F. J.; Sanditov, D. S.; Privalko V. P. *J. Mater. Sci.* **2002**, *37*, 4507.
(52) Oyen, M. L.; Cook, R. F. *J. Mater. Res.* **2003**, *18*, 139.
(53) Min, L.; Wei-Min, C.; Nai-Gang, L.; Ling-Dong, W. *J. Mater. Res.* **2004**, *19*, 73.
(54) Thomas, E. L., Ed. *Materials Science and Technology*; Wiley-VCH: Weinheim, Germany, 1993; Vol. 12.
(55) Fischer Cripps, A. C. *Nanoindentation*; Springer-Verlag: New York, 2002.
(56) Pawlak, A.; Galeski, A. *Macromolecules* **2005**, *38*, 9688.
(57) Bushby, A. J.; Dunstan, D. J. *J. Mater. Res.* **2004**, *19*, 137.
(58) Zhou, Y.; Mallick, P. K. *Polym. Eng. Sci.* **2002**, *42*, 2449.
(59) Robertson, R. E. *J. Appl. Polym. Sci.* **1963**, *7*, 443.
(60) Roetling, J. A. *Polymer* **1965**, *6*, 311.
(61) Kazmierczak, T.; Galeski, A.; Argon, A. S. *Polymer* **2005**, *46*, 8926.
(62) Bartczak, Z.; Galeski, A. *Polymer* **1999**, *40*, 3677.
(63) Bartczak, Z.; Kozanecki, M. *Polymer* **2005**, *46*, 8210.
(64) Bartczak, Z. *Polymer* **2005**, *46*, 10339.
(65) Pluta, M.; Bartczak, Z.; Galeski, A. *Polymer* **2000**, *41*, 2271.
(66) Tranchida, D.; Piccarolo, S. *Macromol. Rapid Commun.* **2005**, *26*, 1800.
(67) Oliver, W. C.; Pharr, G. M. *J. Mater. Res.* **1992**, *7*, 1564.
(68) Loubet, J. L.; Georges, J. M.; Meille, J. *Nanoindentation Techniques in Materials Science and Engineering*; ASTM: Philadelphia, PA, 1986.
(69) Malzbender, J.; de With, G.; den Toonder, J. *J. Mater. Res.* **2000**, *15*, 1209.
(70) Cheng, Y.-T.; Cheng, C. M. *Appl. Phys. Lett.* **1998**, *73*, 614.
(71) Wu, X. Z.; Ocko, B. M.; Sirota, E. B.; Sinha, S. K.; Deutsch, M.; Cao, B. H.; Kim, M. W. *Science* **1993**, *261*, 1018.
(72) Liu, Y.; Russell, T. P.; Samant, M. G.; Stohr, J.; Brown, H. R.; Cossy-Favre, A.; Diaz, J. *Macromolecules* **1997**, *30*, 7768.
(73) Xie, L.; DeMaggio, G. B.; Frieze, W. E.; DeVries, J.; Gidley, D. W.; Hristov, H. A.; Yee, A. F. *Phys. Rev. Lett.* **1996**, *74*, 4947.
(74) Tsui, O. K. C.; Wang, X. P.; Ho, J. Y. L.; Ng, T. K.; Xiao, X. *Macromolecules* **2000**, *33*, 4198.
(75) Kaijiama, T.; Tanaka, K.; Takahara, A. *Macromolecules* **1995**, *28*, 3482.
(76) Hammerschmidt, J. A.; Gladfelter, W. L.; Haugstad, G. *Macromolecules* **1999**, *32*, 3360.

MA052727J